Chinese Chemical Letters 37 (2026) 112027

Contents lists available at ScienceDirect

Chinese Chemical Letters

journal homepage: www.elsevier.com/locate/cclet

Exosome-liposome hybrid system with antioxidant and anti-inflammatory activities targeting glial cells for the treatment of central nervous system diseases

Yutong Chen[a,1], Shuting Guo[a,1], Mingrui Fan[a], Songlin Yang[a], Qiuxia Lin[a], Jiafeng Zou[a], Junyuan Xu[a], Tongtong Zheng[a], Kangtai He[a], Feng Gao[a,b,c], Yanzuo Chen[a,b,*]

[a] Pharmaceutical Engineering and Process of Chemical Engineering Research Center of Ministry of Education, Shanghai Key Laboratory of New Drug Design, School of Pharmacy, East China University of Science and Technology, Shanghai 200237, China
[b] Optogenetics and Synthetic Biology Interdisciplinary Research Center, State Key Laboratory of Bioreactor Engineering, East China University of Science and Technology, Shanghai 200237, China
[c] Shanghai Key Laboratory of Functional Materials Chemistry, East China University of Science and Technology, Shanghai 200237, China

ARTICLE INFO

Article history:
Received 25 July 2025
Revised 23 October 2025
Accepted 27 October 2025
Available online 28 October 2025

Keywords:
Central nervous system disease
Glial cells
Exosome-liposome hybrid system
Fisetin
Pioglitazone

ABSTRACT

Central nervous system diseases (CNSDs), such as Parkinson's disease (PD) and depression, have attracted considerable attention due to their high morbidity and mortality rates. Neuronal damage in CNSDs is primarily driven by inflammation and oxidative stress induced by activated astrocytes and microglia. Thus, new therapeutic strategies are urgently needed that not only enable effective drug delivery across the blood-brain barrier (BBB), but also specifically target lesions while exerting antioxidant and anti-inflammatory effects on glial cells. To address this challenge, we developed an exosome-liposome hybrid system targeting glial cells co-loaded with fisetin (FIS) and pioglitazone (PIO) (RMP7-EL-FIS-PIO). This hybrid system crosses the BBB through the B2 bradykinin receptor-mediated opening and takes advantage of the homing properties of exosomes to accumulate at the site of brain lesions in murine models of PD and of depression. Through receptor-ligand binding and phagocytosis, the hybrid system targets glial cells to deliver drugs that inhibit their activation, thus protecting neurons. Our study demonstrates the great potential of the developed exosome-liposome hybrid system for the targeted treatment of CNSDs.

© 2026 Published by Elsevier B.V. on behalf of Chinese Chemical Society and Institute of Materia Medica, Chinese Academy of Medical Sciences.

Central nervous system diseases (CNSDs), including neurodegenerative diseases and cognitive disorders, affect approximately one-sixth of the global population [1,2]. Among the more prevalent chronic CNSDs, Parkinson's disease (PD) and depression are characterized by ongoing neuronal damage to specific regions of the brain [3–5]. Unfortunately, current treatment approaches, such as neurotransmitter modulation, stem cell transplantation, and deep brain stimulation, are unable to prevent the continuous loss of neurons [6,7]. Thus, it is crucial to develop comprehensive treatment strategies aimed at protecting neurons in patients with CNSDs.

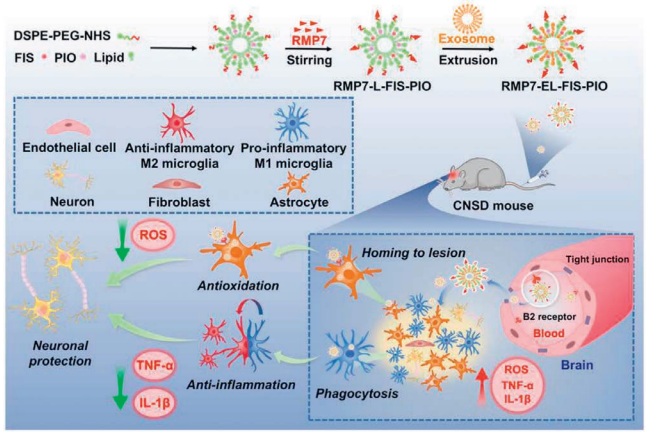
Oxidative stress and inflammation drive excessive accumulation of reactive oxygen species (ROS) and infiltration of peripheral immune cells into the brain parenchyma, both of which hinder neuronal recovery in CNSDs [8–10]. This process also triggers the activation of astrocytes, which serve as vital reservoirs of antioxidants for neurons, leading to the overproduction of ROS [11], which in turn lead to breakdown of the plasma membrane and protein deposition, ultimately triggering neuronal apoptosis [12]. As a natural polyphenolic flavonoid with potent free radical scavenging properties, fisetin (FIS) inhibits cell proliferation and migration in different cell types [13,14]. Thus, targeted delivery of FIS to sites of brain injury may help to suppress activation of astrocytes, thereby promoting neuronal survival and recovery. However, during neuroinflammation, damage-associated molecular patterns released by neurons can recruit and polarize microglia into the M1 phenotype, which secretes neurotoxic cytokines, such as interleukin (IL)-1β and tumor necrosis factor (TNF)-α [15]. This suggests that merely inhibiting oxidative damage may not be sufficient for the treatment of CNSDs. Pioglitazone (PIO), a clinical antidiabetic agent, also exhibits neuroprotective effects by polarizing M1 microglia into the anti-inflammatory M2 phenotype [16]. Combining PIO with FIS to inhibit glial cell activation in the brain may offer a more effective strategy for the treatment of CNSDs.

* Corresponding author.
E-mail address: chenyz@ecust.edu.cn (Y. Chen).
[1] These authors contributed equally to this work.

https://doi.org/10.1016/j.cclet.2025.112027
1001-8417/© 2026 Published by Elsevier B.V. on behalf of Chinese Chemical Society and Institute of Materia Medica, Chinese Academy of Medical Sciences.

FIS and PIO are insoluble drugs with asynchronous biodistribution and limited permeability across the blood-brain barrier (BBB), which hampers their accumulation at lesion sites and reduces their therapeutic efficacy [17,18]. The primary obstacle to BBB penetration is the tight junctions located between brain microvascular endothelial cells (BMECs) [19]. Activation of B2 bradykinin receptors on BMECs promote cytoskeletal contractility, which facilitate the opening of these tight junctions [20]. However, the plasma half-life of bradykinin is <1 min because of the susceptibility of its peptide bonds to enzymatic degradation. Furthermore, hydrolysis of these peptide bonds diminishes the affinity of bradykinin for B2 receptors, limiting its ability to cross the BBB. To overcome these limitations, a bradykinin analogue, Cereport (receptor-mediated permeabilizer-7 (RMP-7)), was developed [21]. By introducing enzymatically resistant synthetic amino acids and reducing peptide bonds, RMP-7 exhibits an extended half-life and enhanced binding affinity for B2 receptors, thereby facilitating a more sustained opening of the BBB [22,23]. Consequently, RMP-7 modified nanoparticles may improve drug accumulation in the brain parenchyma. At the site of CNSDs lesions, the prolonged inflammatory response often results in an increase in chemotactic cytokines, which subsequently recruit fibroblasts to form fibrous scars [24]. Consequently, fibroblast-derived exosomes, which carry homologous surface proteins inherited from their source cells, are ideal candidates for developing lesion site-specific drug delivery systems [25]. Similarly, liposomes, which are nanodrug delivery systems with a lipid bilayer structure similar to that of exosomes, exhibit high biocompatibility and excellent drug loading capacity [26,27]. As a result, hybrid systems that combine liposomes and exosomes exhibit enhanced drug loading and homologous targeting capabilities. Thus, a RMP7-modified exosome-liposome (RMP7-EL) hybrid system is a promising strategy for the efficient and concurrent delivery of FIS and PIO, capable of crossing the BBB and accumulating at the site of the injury.

In this study, an RMP7-EL hybrid system co-loaded with FIS and PIO (RMP7-EL-FIS-PIO) was developed to exert antioxidant and anti-inflammatory activities to protect brain neurons. As illustrated in Scheme 1, the RMP7-EL-FIS-PIO hybrid system was prepared using the membrane extrusion method. Extrusion-induced mechanical stress causes transient membrane destabilization in both liposomes and exosomes, facilitating close membrane contact [28,29]. Following intravenous administration to CNSDs mice, RMP7-EL-FIS-PIO crossed the BBB through the B2 bradykinin receptor-mediated opening of tight junctions. Once in the brain, the exosome-liposome hybrid system homed to the site of the lesion due to the exosome component, where it was subsequently endocytosed by glial cells, specifically astrocytes that are characterized by high expression of the B2 bradykinin receptor, and microglia. The hybrid system effectively exploited the properties of FIS and PIO to inhibit glial cell activation through ROS scavenging and promoted the polarization of M2 microglia, thus providing neuroprotection. Our findings demonstrated the efficacy and safety of the RMP7-EL-FIS-PIO hybrid system in alleviating behavioral abnormalities in murine models of PD and of depression. Hence, the RMP7-EL hybrid system holds promise as a novel therapeutic strategy for CNSDs.



Scheme 1. Schematic illustration of the therapeutic strategy of the RMP7-EL-FIS-PIO hybrid system. RMP7-EL-FIS-PIO were prepared by extruding exosomes with RMP7-L-FIS-PIO. In murine models of CNSDs, RMP7-EL-FIS-PIO open the tight junctions of the BBB, home and accumulate at the lesion sites, and deliver FIS and PIO to astrocytes and microglia to exert antioxidant and anti-inflammatory activities, thereby protecting neurons by inhibiting glial cell activation.

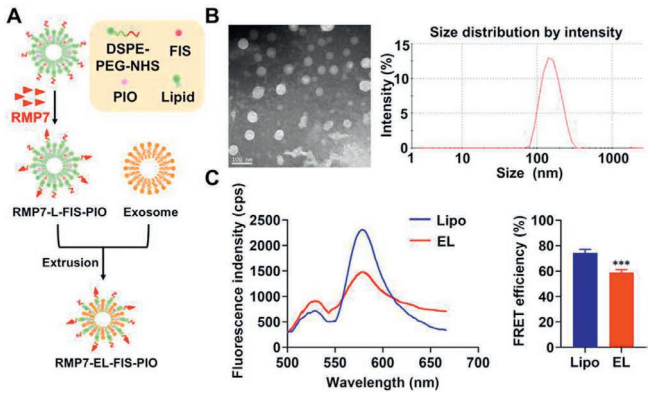


Fig. 1. Characterization of RMP7-EL-FIS-PIO. (A) Schematic illustration of the preparation of RMP7-EL-FIS-PIO. (B) Transmission electron microscopy (TEM) image and size distribution of RMP7-EL-FIS-PIO. Scale bar: 100 nm. (C) FRET study of nanoparticles labeled with fluorescent donor NBD (λ_{em} = 525 nm) and fluorescent acceptor RhB (λ_{em} = 595 nm) at an excitation wavelength of 488 nm. Data are presented as mean ± standard deviation (SD) (n = 5). $^{***}P < 0.001$.

RMP7-EL-FIS-PIO was prepared by membrane fusion, as illustrated in Fig. 1A. Both the L-929-derived exosomes and liposomes presented vesicular structures, with an average particle size of 108.6 nm and 162.2 nm, respectively (Fig. S1 in Supporting information). RMP7-EL-FIS-PIO presented a spherical morphology, with a hydrodynamic diameter of 134.1 ± 1.7 nm (polydispersity index 0.15) and a zeta potential of −2.9 ± 0.25 mV (Fig. 1B). The membrane fusion of exosome and liposome was validated by the fluorescence resonance energy transfer (FRET) assay. Insertion of exosome into the lipid bilayer of the FRET liposome increased the distance between the fluorescence donor L-α-phosphatidylethanolamine-*N*-(4-nitrobenzo-2-oxa-1,3-diazole) (ammonium salt) (PE-NBD) and fluorescent acceptor PE-(lissamine rhodamine-B sulfonyl) (ammonium salt) (PE-RhB), thus decreasing the emission peak intensity of PE-RhB (Fig. 1C), suggesting the successful hybridization of exosome and liposome. Moreover, the protein composition in the exosome was mostly retained in EL-FIS-PIO (Fig. S2 in Supporting information), but no protein signal was detected in L-FIS-PIO, suggesting that the hybrid system retained the biological functions of exosomes. The coupling efficiency of RMP7 on the liposome surface was 73.8 %, whereas the encapsulation efficiency of FIS and PIO in RMP7-EL-FIS-PIO was 83.6 % ± 2.7 % and 63.6 % ± 1.5 %, respectively. The drug loading capacities were 2.9 % ± 0.8 % and 1 % ± 0.4 %, respectively. After one week of storage, no changes in appearance, particle size, zeta potential, or drug loading were observed, indicating that RMP7-EL-FIS-PIO was physically stable. The release of FIS and PIO from RMP7-EL-FIS-PIO followed uniform release kinetic curves (Fig. S3 in Supporting information), with 90.2 % and 86.6 % of drug released within 72 h, respectively. These findings demonstrate the synchronous behavior of the two drugs, which may enhance their combined therapeutic effect.

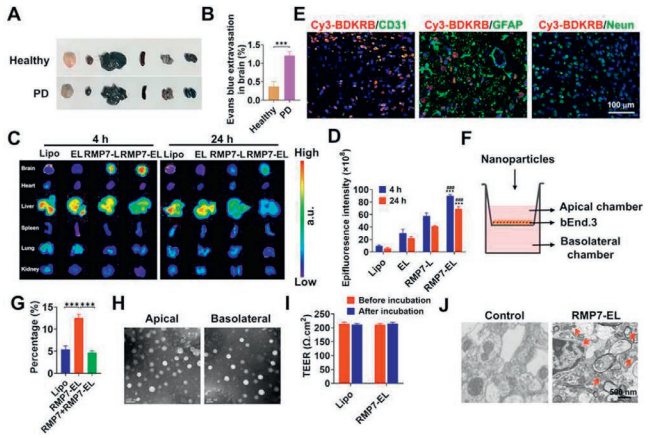


Fig. 2. Brain-targeting and BBB permeability of RMR7-EL. Mice were intravenously injected with 2 % Evans blue: (A) Photographs of the major organs 8 h after administration, and (B) Evans blue quantification of brain tissues ($n = 5$). Murine models of PD were intravenously administered with 2 % DiD-labeled nanoparticles, in (C) *ex vivo* fluorescence images of major organs, and in (D) fluorescence quantification in brain tissues ($n = 3$). (E) Fluorescence images of the expression of Cy3-BDKRB-labeled B2 bradykinin receptors on CD31-stained BMEC, GFAP-stained astrocytes, and neuronal nuclei (Neun)-stained neurons in brain tissues. Scale bar: 100 μm. (F) Schematic illustration of the *in vitro* BBB penetration test. (G) The fluorescence intensity ratio of the lower chamber *versus* the upper chamber after a 4-h incubation ($n = 5$). (H) Transmission electron microscopy (TEM) images of the medium collected from the apical and basolateral chambers after treatment with RMP7-EL. Scale bar: 100 nm. (I) TEER of the monolayer bEnd.3 cells before and after treatment ($n = 3$). (J) TEM images of the substantia nigra of murine models of PD 12 h after intravenous administration of RMP7-EL. Red arrows indicate nanoparticles. Scale bar: 500 nm. Data are presented as mean ± SD. $^{***}P < 0.001$ *vs.* the liposome group, $^{\#\#\#}P < 0.001$ *vs.* the EL group.

The integrity of the BBB of PD mice was assessed by extravasation of albumin-conjugated Evans blue dye [30]. All animal experiments were performed in accordance with guidelines approved by the Ethics Committee of East China University of Science and Technology (the approval No. SCXK 2023–0004). The content of Evans blue in the brain of PD mice was 2.1-fold higher than that of healthy mice ($P < 0.001$, Figs. 2A and B), indicating increased BBB permeability, which may attribute to the disruption of endothelial tight junctions caused by excessive oxidative stress and inflammation [31]. However, 4 h after administration of the DiD-labeled liposome, the fluorescence intensity of the brain-to-liver ratio was 0.04 (Figs. 2C and D), suggesting that most of the nanoparticles were hindered by the tight junctions between endothelial cells. Unlike liposomes, the accumulation of EL was decreased in the liver, suggesting that exosomal hybridization reduced the clearance of nanoparticles by the reticuloendothelial system, resulting from the expression of the CD47 protein as a "don't eat me" signal [32]. However, no obvious differences were observed in brain accumulation between the EL and liposome groups, indicating that EL was inadequate for brain targeting. Although, after modification of RMP7, the fluorescence intensity of the hybrid nanoparticles in the brain was 2.2 times higher ($P < 0.001$), suggesting a greater accumulation of RMP7-EL in the brain parenchyma. As a B2 bradykinin receptor agonist, RMP7 rearranges cytoskeletal proteins and downregulates proteins related to tight junctions, transiently increasing BBB permeability and thus improving nanoparticle accumulation in the brain parenchyma [33]. B2 bradykinin receptors are expressed in brain microvascular endothelial cells (labeled with CD31) and astrocytes (expressing glial fibrillary acidic protein (GFAP)) but are expressed at low levels in neurons (Fig. 2E). Therefore, RMP7-EL may specifically target astrocytes after crossing the BBB. Furthermore, liposome, EL, and RMP7-EL exhibited negligible neuronal cytotoxicity even at concentrations as high as 200 μg/mL (Fig. S4A in Supporting information), indicating favorable biosafety.

The integrity of nanoparticles after crossing the BBB is essential for the delivery of cargo to the PD lesion, and therefore a Transwell assay using the bEnd.3 brain microvascular endothelial cell line was seeded in the apical chamber, as illustrated in Fig. 2F. In the basolateral chamber, the RMP7-EL exhibited a 1.3-fold increase in fluorescence intensity compared to the liposome alone ($P < 0.001$, Fig. 2G) with spherical structures closely resembling those of the apical chamber (Fig. 2H), indicating the potential of RMP7-EL to cross the BBB without losing its integrity. Furthermore, after treatment with RMP7-EL, the cell monolayer remained intact with transendothelial electrical resistance (TEER) of over 200 $\Omega\,cm^2$ (Fig. 2I), suggesting that the increased permeability was achieved through transient open junctions between endothelial cells [34]. Furthermore, nanometer-sized vesicles with a more uniform distribution were found in the substantia nigra of PD mice than that of healthy mice (Fig. 2J), confirming that RMP7-EL reached the brain injury site in the form of nanoparticles. Overall, with combined brain targeting and BBB crossing capability, RMP7-EL exhibited the potential to deliver drugs to the brain parenchyma of CNSDs.

To determine whether nanoparticles could deliver drugs to astrocytes and microglia at the site of the lesion, the distribution of DiD-labeled nanoparticles in the brain was studied. RMP7-EL showed stronger fluorescence than RMP7-L, especially in the substantia nigra ($P < 0.001$, Figs. 3A and B). In the PD brain, the number of α-smooth muscle actin (α-SMA)-positive fibroblasts and fibronectin were obviously greater compared to healthy mice (Fig. S5 in Supporting information), indicating the formation of fibrotic scars in the substantia nigra. These findings indicated that fibroblast-derived exosomes can target brain lesion sites through their homologous targeting ability [35,36]. Thus, a drug delivery system based on fibroblast-derived exosomes was able to target the lesion site due to homologous surface adhesion proteins [37].

Most CNSDs exhibit activated astrocytes and microglia in areas of brain damage [38], and therefore the distribution of RMP7-EL in the substantia nigra of PD mice was further studied. Limited colocalization of DiD-labeled nanoparticles with astrocytes (labeled with GFAP) and microglia (labeled with Iba1) was observed (Figs. 3C and D), whereas the yellow region overlapped expanded after RMP7 modification. In particular, RMP7-EL showed 2.3- and 3.5-fold more colocalization to astrocytes and microglia

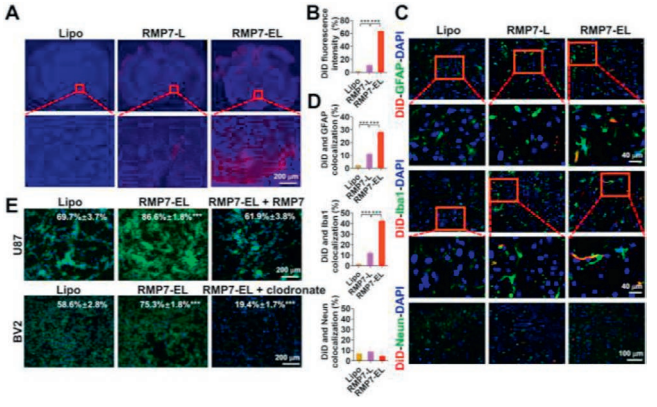


Fig. 3. RMP7-EL targets astrocytes and microglia. PD mice received intravenous injection of DiD-labeled nanoparticles. Four hours after administration, brains were dissected and sectioned. (A) Immunofluorescent images of brain tissues and (B) quantification of the fluorescence intensity in the substantia nigra. Red boxes indicate the substantia nigra. (C) Immunofluorescent images of the substantia nigra, with astrocyte stained with GFAP, microglia stained with Iba1, and neurons stained with Neun, and (D) quantification. Scale bar: 100 μm. Red boxes indicate the representative region of the substantia nigra. (E) Fluorescence images of U87 and BV2 cells after 4-h incubation with C6-labeled nanoparticles. Scale bar: 200 μm. Data are presented as mean ± SD ($n = 5$). $^{***}P < 0.001$ *vs.* the liposome group.

than RMP7-L, respectively ($P < 0.001$), resulting from exosomal homing to the substantia nigra. Similarly, less RMP7-EL colocalized with neurons. Furthermore, RMP7-EL absent in the glial cells of healthy mice (Fig. S6 in Supporting information), confirming its specific targeting of the PD site. To investigate the targeting mechanism of RMP7-EL in glial cells, the cellular uptake of U87 astrocytes and BV2 microglia of C6-labeled nanoparticles was studied. The fluorescence intensity of the RMP7-EL group was much higher than that observed in the RMP7-pretreatment and liposome groups (Fig. 3E), suggesting that increased astrocyte uptake was due to binding of RMP7 and B2 bradykinin receptors. In contrast, microglial uptake of RMP7-EL was inhibited by the phagocytic inhibitor clodronate, indicating that the nanoparticles were internalized by microglia by phagocytosis. More importantly, the cytotoxicity of RMP7-EL-FIS-PIO was significantly lower than that of free drugs, with an half-maximal inhibitory concentration (IC_{50}) value of 39.01 μg/mL (Fig. S4B in Supporting information), ensuring its biosafety *in vivo*. Collectively, RMP7-EL has the ability to cross the BBB, reach lesion sites, and target glial cells, making it highly promising for the treatment of CNSDs.

Neuronal damage in the brain is primarily related to activate glial cell-induced inflammation and oxidative stress [39]. In CNSDs, excessive ROS cause oxidative stress and mitochondrial dysfunction, culminating in neuronal damage and death [40]. Therefore, the ROS scavenging effect of RMP7-EL-FIS-PIO on U87 astrocytes was evaluated by detection of markers related to oxidative stress. After stimulation by 1-methyl-4-phenyl-1,2,3,6-tetrahydropyridine (MPTP), a mitochondrial complex 1 inhibitor, ROS levels increased significantly in U87 astrocytes (Figs. 4A and B) but decreased after treatment with either single or dual drug-loaded nanoparticles. Similarly, RMP7-EL-FIS and RMP7-EL-PIO decreased ROS levels in the substantia nigra by 1.9- and 1.6-fold compared with phosphate-buffered saline (PBS) treatment, respectively, whereas RMP7-EL-FIS-PIO treatment achieved the greatest reduction in ROS levels of 5.4-fold ($P < 0.001$, Figs. 4C and D). The decline in ROS levels may have been due to the combined effects of FIS and PIO, which promoted the restoration of oxidative balance and blocked the vicious cycle of inflammation and oxidative stress. The lipid peroxidation product, malondialdehyde, measured 11.2 nmol/mgprot in the RMP7-EL-FIS-PIO treated group, and was lower than that detected following PBS treatment (19.2 nmol/mgprot, $P < 0.001$, Fig. 4E). Furthermore, the RMP7-EL-FIS-PIO hybrid system increased the levels of the representative endogenous antioxidant enzyme, superoxide dismutase, in the brain of PD by 1.3-fold compared with the PBS group (Fig. 4F), suggesting suppression of oxidative stress. In particular, RMP7-EL-FIS significantly reduced ROS and malondialdehyde levels by 47 % and 36 %, respectively, and doubled superoxide dismutase levels ($P < 0.001$). In contrast, improvements in these oxidative stress indices were less pronounced in the RMP7-EL-PIO treatment group, suggesting that FIS was the main component exerting antioxidant effects in the hybrid system, possibly related to its role as a natural flavonoid with the ability to neutralize free radicals [41]. Thus, the exosome-liposome hybrid system was beneficial in protecting brain neurons from damage caused by oxidative stress and has the potential to increase their survival.

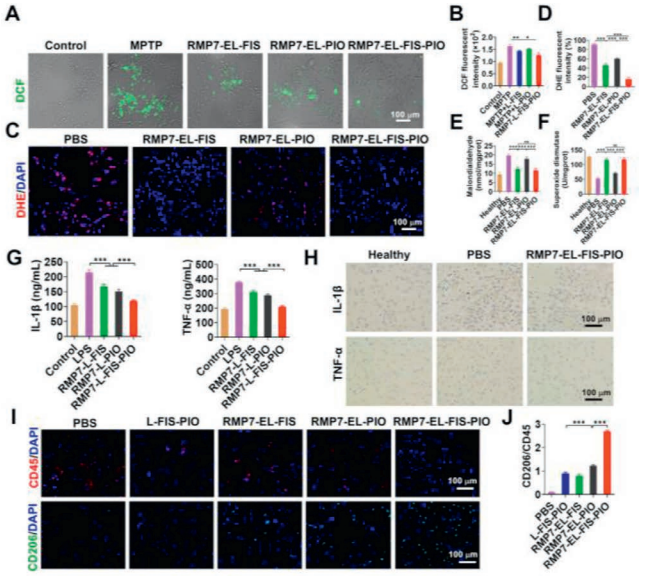


Fig. 4. Antioxidant and anti-inflammatory effects of RMP7-EL-FIS-PIO. (A) Fluorescence images of ROS levels in U87 cells after a 2-h incubation with nanoparticles and (B) relative quantification ($n = 3$). (C) Representative images of ROS staining in the substantia nigra of PD mice 24 h after five intravenous injections of RMP7-EL-FIS-PIO and (D) quantification ($n = 5$). Concentrations of (E) malondialdehyde and (F) superoxide dismutase in brain tissues ($n = 5$). (G) IL-1β and TNF-α levels in BV2 cells 24 h after different treatments ($n = 5$). (H) Immunohistochemical staining of IL-1β and TNF-α in the brain of PD mice. (I) Immunofluorescence images of CD45-positive M1 microglia and CD206-positive M2 microglia. Scale bar: 100 μm. (J) The M2/M1 ratio ($n = 5$). Data are presented as mean ± SD. $^{*}P < 0.05$, $^{**}P < 0.01$, $^{***}P < 0.001$.

In CNSDs, the inflammatory response is primarily caused by the activation and migration of microglia [42]. The *in vitro* anti-inflammatory efficacy of the RMP7-EL-FIS-PIO hybrid system was evaluated using lipopolysaccharide (LPS)-activated BV2 microglia. After treatment with RMP7-modified nanoparticles, the levels of IL-1β and TNF-α were reduced by ~1.8-fold, compared with LPS-induced inflammatory microglia ($P < 0.001$, Fig. 4G). Similarly, IL-1β and TNF-α levels in the substantia nigra of PD mice were significantly reduced after treatment with the RMP7-EL-FIS-PIO hybrid system (Fig. 4H), indicating a strong anti-inflammatory effect. In brain regions associated with PD, microglia are predominantly polarized into the pro-inflammatory M1 phenotype, whereas the M2 phenotype of microglia helps mitigate inflammation and neuronal damage [43]. The M2/M1 ratio in the RMP7-EL-FIS-PIO treatment group was 2.7 (Figs. 4I and J), which was higher than that observed in the RMP7-EL-FIS and RMP7-EL-PIO groups ($P < 0.001$), suggesting that RMP7-EL-FIS-PIO may have had a higher therapeutic efficacy for PD. The RMP7-EL-FIS-PIO hybrid system achieved an enhanced anti-inflammatory effect, mainly because FIS restores redox homeostasis, which helps maintain the resting state of microglia, and PIO promotes the polarization of microglia toward the M2 phenotype. Taken together, the nanoparticle RMP7-EL-FIS-PIO may be beneficial for the treatment of PD due to its superior antioxidant and anti-inflammatory properties.

Lipophilic MPTP not only crosses the BBB, but its metabolites can also damage dopaminergic neurons and induce PD [44]. Therefore, a MPTP-induced murine model of PD was established to evaluate the therapeutic effects of RMP7-EL-FIS-PIO (Fig. 5A). After treatment, the rotarod test, pole test, and cylinder test were conducted to study the movement and exploration capacity of PD mice [45,46]. As shown in Fig. 5B and Fig. S7 (Supporting information), compared with healthy mice, PD mice showed obvious motor dysfunction, as evidenced by the increased total time required to reach the bottom and the time to turn (T-turn), as well as the decrease in latency time and distance. After treatment with RMP7-EL-FIS-PIO, these indicators improved significantly ($P < 0.001$), with total time and T-turn values of 8.8 and 2.1 s, respectively, which were lower than those of the control group (13.4 and 4.0 s), whereas the retention time and distance were prolonged, suggesting the restoration of motor dysfunction in PD model mice. Furthermore, PD mice tended to avoid exploring unfamiliar environments by reducing the use of their forelimbs [46], resulting in a lower frequency of forelimb outstretching within 3 min compared to healthy mice, 8 *vs.* 19 times ($P < 0.001$, Fig. 5C). After treatment with the RMP7-EL-FIS-PIO hybrid system, the frequency of forelimb

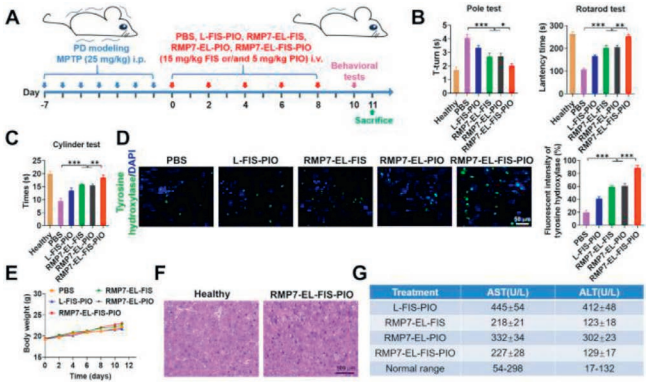


Fig. 5. Anti-PD efficacy and biosafety of the RMP7-EL-FIS-PIO hybrid system. (A) The establishment of the MPTP-induced murine model for PD and murine model treatment schedule. (B) Time required for the mice to orient downward at the top of a vertical pole (T-turn) and latency time on the rotarod ($n = 3$). (C) Number of forelimb outstretches in 3 min ($n = 3$). (D) Representative images and quantification of tyrosine hydroxylase staining in the substantia nigra ($n = 5$). Scale bar: 50 μm. (E) Changes in body weight of PD model mice ($n = 3$). (F) Hematoxylin-eosin (H&E) staining of the substantia nigra. (G) Serum levels of ALT and AST ($n = 3$). Scale bar: 100 μm. Data are presented as mean ± SD. $^{*}P < 0.05$, $^{**}P < 0.01$, $^{***}P < 0.001$.

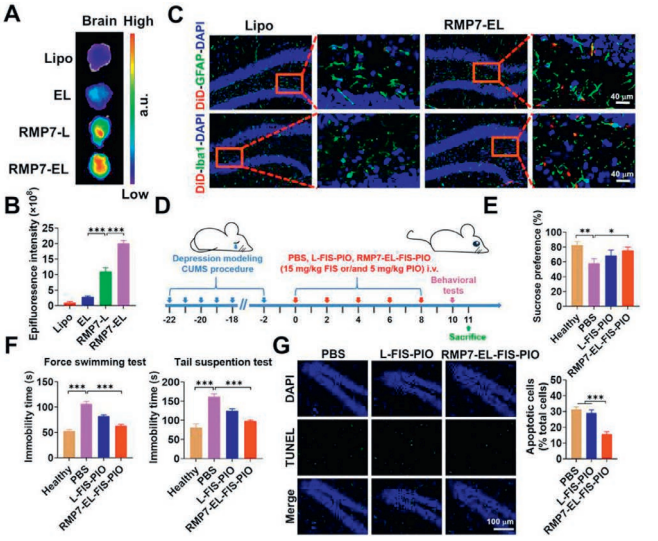


Fig. 6. Effects of RMP7-EL-FIS-PIO in depression mice. Murine models of depression received 2 % DiD-labeled nanoparticles administered intravenously. Four hours after administration, the brains were dissected and sectioned. (A) *Ex vivo* fluorescence images of brain tissues and (B) quantification ($n = 3$). (C) Fluorescence colocalization images of DiD-labeled nanoparticles with astrocytes and microglia. Red boxes indicate the representative region of the hippocampus. Scale bar: 100 μm. (D) The establishment of the murine model of CUMS-induced depression and the treatment schedule. (E) Sucrose preference test, (F) immobility time under forced swimming and tail suspension stressors ($n = 3$). (G) Terminal deoxynucleotidyl transferase dUTP nick end labeling (TUNEL) staining of brain sections and quantitation ($n = 5$). Scale bar: 100 μm. Data are presented as mean ± SD. $^{*}P < 0.05$, $^{**}P < 0.01$, $^{***}P < 0.001$.

outstretching (17 times) was comparable to that of the healthy mice group (19 times) and was significantly higher than that of the nanoparticle treatment groups loaded with single drug ($P < 0.01$), which indicated that behavioral abnormalities were alleviated. Tyrosine hydroxylase, a key rate-limiting enzyme in dopamine synthesis [47], was expressed at low levels in the substantia nigra of PD model mice (Fig. 5D). After treatment with the RMP7-EL-FIS-PIO hybrid system, the expression of tyrosine hydroxylase increased by 4.6- and 1.5-fold compared with treatment with PBS and the single drug-loaded nanoparticles, respectively ($P < 0.001$), indicating potent neuroprotective effects. The satisfactory efficacy may be due to the synergistic effects of FIS and PIO in improving the cerebral microenvironment, resulting in promoting the expression of neurotrophic factors and the differentiation of neural stem cells, thereby augmenting neuronal activity in the motor cortex [48–50].

During treatment, the body weight of the mice in all groups increased steadily, and no obvious histological damage was observed in the substantia nigra (Figs. 5E and F). This result may be due to the ability of nanoparticles to target the substantia nigra, thus avoiding injury to normal brain cells caused by offsite the distribution throughout the entire brain. The metabolism of PIO may induce oxidative imbalance by glutathione depletion [51]; thus, the liver function markers alanine aminotransferase (ALT) and aspartate aminotransferase (AST) were examined. After treatment with L-FIS-PIO and RMP7-EL-PIO, AST, and ALT levels in the serum of mice were markedly elevated (Fig. 5G), whereas after treatment with RMP7-EL-FIS and RMP7-EL-FIS-PIO, transaminase levels remained within the normal range. Furthermore, the liver morphology was similar to that of a healthy liver after treatment with the RMP7-EL-FIS-PIO hybrid system (Fig. S8 in Supporting information), indicating that the combination with FIS can protect hepatocytes from oxidative damage caused by PIO through its ability to maintain intracellular redox homeostasis. Furthermore, the dose of PIO was reduced to one-third of the standard dose of 15 mg/kg [52], further reducing the risk of liver injury. Taken together, the RMP7-EL-FIS-PIO hybrid system was found to be effective and safe for the treatment of PD.

Depression is a common mood disorder affecting ~3 %–5 % of the global population, characterized by the activation of glial cells and the loss of neurons in the hippocampus [53–55]. A murine model of chronic unpredictable mild stress (CUMS)-induced depression was used to evaluate the brain targeting ability and the therapeutic effects of RMP7-EL-FIS-PIO. Four hours after administration, RMP7-EL showed higher brain accumulation in mice compared with EL and RMP7-L ($P < 0.001$, Figs. 6A and B). In particular, RMP7-EL accumulated ~6.6-fold more in the hippocampus compared with liposomes and showed a greater degree of colocalization with astrocytes and microglia (Fig. 6C), suggesting that RMP7-EL was more effective in delivering drugs to glial cells rather than to neurons. The results were consistent with those of the murine models with PD, indicating that RMP7-EL has a good drug-targeting delivery capacity for the treatment of CNSDs characterized by activation of astrocytes and microglia.

Next, the antioxidant and anti-inflammatory effects of RMP7-EL-FIS-PIO were studied in murine models of depression. As shown in Fig. S9 (Supporting information), the oxidative stress factor ROS were elevated in the PBS group but decreased by 8.1-fold after treatment with the RMP7-EL-FIS-PIO hybrid system (Fig. S9A); similarly, malondialdehyde decreased significantly from 19.8 nmol/mg to 12.3 nmol/mg ($P < 0.001$, Fig. S9B), whereas the level of superoxide dismutase increased 2.2-fold (Fig. S9C). Meanwhile, the inflammatory factors IL-1β and TNF-α were markedly down-regulated in the group treated with RMP7-EL-FIS-PIO (Fig. S9D). The M2/M1 ratio in the RMP7-EL-FIS-PIO group was significantly higher than that in the L-FIS-PIO group ($P < 0.001$, Figs. S9E and F), indicating a good microglia polarization capacity. The excellent antioxidant and anti-inflammatory results suggested that the drug delivery system may have a good therapeutic effect on depression.

The treatment scheme for the CUMS-induced depression model mice is illustrated in Fig. 6D. Following 3-week stimulation, depressed mice lost interest in sweets with a sucrose preference value of 56.3 % (Fig. 6E). Although after treatment with RMP7-EL-FIS-PIO, this value increased to 76.7 % ($P < 0.05$), possibly due to improvements in the brain reward circuit that restored hedonic capacity [56]. Depressed mice also exhibited behavioral despair, with

a prolonged immobility time in the FST (101 s) and TST (157 s), which were reduced by 34 % and 43 %, respectively, after treatment with RMP7-EL-FIS-PIO ($P < 0.001$, Fig. 6F), suggesting that the drug delivery system alleviated despair depressive behavior. Furthermore, the significant pathological manifestation of depression, neuronal apoptosis, was significantly reduced after treatment with RMP7-EL-FIS-PIO ($P < 0.001$, Fig. 6G), which may be attributed to the increased distribution of nanoparticles in the hippocampal region, particularly in the dentate gyrus (Fig. 6C). The dentate gyrus serves as the primary recipient of cortical input and is considered a key region for hippocampal neurogenesis. Furthermore, RMP7-EL-FIS-PIO treatment showed good safety with serum AST and ALT levels within the normal range (Table S2 in Supporting information). In conclusion, RMP7-EL-FIS-PIO may be considered effective and safe for the treatment of CNSDs with astrocyte and microglia activation.

In this study, we developed RMP7-EL-FIS-PIO, an RMP7-modified exosome-liposome hybrid system co-loaded with FIS and PIO, aimed at alleviating brain neuronal damage. The hybrid system effectively crossed the BBB and inhibited glial cell activation, thus exerting antioxidant and anti-inflammatory activities. Treatment with the hybrid system RMP7-EL-FIS-PIO achieved satisfactory neuroprotective effects and alleviated behavioral abnormalities in murine models of PD and depression. Furthermore, RMP7-EL-FIS-PIO did not exhibit any obvious systemic toxicity. Overall, these findings highlight that the RMP7-modified exosome-liposome hybrid system is a promising brain-targeted drug delivery strategy with substantial potential for the treatment of CNSDs.

CRediT authorship contribution statement

Yutong Chen: Writing – review & editing, Methodology, Investigation, Data curation. **Shuting Guo:** Methodology, Investigation, Formal analysis. **Mingrui Fan:** Writing – review & editing, Methodology, Investigation. **Songlin Yang:** Investigation, Data curation. **Qiuxia Lin:** Methodology, Investigation, Formal analysis. **Jiafeng Zou:** Methodology, Formal analysis. **Junyuan Xu:** Investigation, Formal analysis. **Tongtong Zheng:** Methodology, Investigation. **Kangtai He:** Investigation, Data curation. **Feng Gao:** Supervision, Project administration. **Yanzuo Chen:** Writing – review & editing, Supervision, Project administration, Funding acquisition, Conceptualization.

Declaration of competing interest

The authors declare that they have no known competing financial interests or personal relationships that could have appeared to influence the work reported in this paper.

Acknowledgments

This work was supported by Development Program of China (No. 2019YFA0904800), Shanghai Frontiers Science Center of Optogenetic Techniques for Cell Metabolism, Science and Technology Commission of Shanghai Municipality (No. 10DZ2220500), Shanghai Committee of Science and Technology (No. 11DZ2260600).

Supplementary materials

Supplementary material associated with this article can be found, in the online version, at doi:10.1016/j.cclet.2025.112027.

References

[1] X. Zhou, Q.R. Smith, X. Liu, Wiley Interdiscip. Rev. Nanomed. Nanobiotechnol. 13 (2021) e1695.
[2] Q. Zhang, Q. Jiang, K. Sa, et al., Phytother. Res. 37 (2023) 4885–4907.
[3] Z. Vahidinia, S. Barati, A. Azami Tameh, et al., Neuropeptides 107 (2024) 102451.
[4] L. Jin, J. Zhang, L. Nie, et al., Chin. Chem. Lett. 36 (2025) 110774.
[5] T. Liu, X. Han, X. Sun, et al., Chin. Chem. Lett. 36 (2025) 111170.
[6] L.L. Ji, T.T. Huang, L.L. Mao, et al., Kaohsiung J. Med. Sci. 39 (2023) 1002–1010.
[7] H. Adachi, A. Morizane, S. Torikoshi, et al., Stem Cells Transl. Med. 11 (2022) 767–777.
[8] X. Tang, P. Deng, Y. Jiang, et al., Biomedicines 11 (2023) 2878.
[9] H.S. Díaz, A. Ríos-Gallardo, D. Ortolani, et al., Antioxidants 11 (2022) 1928.
[10] K. Ge, Z. Li, A. Wang, et al., ACS Nano 17 (2023) 2222–2234.
[11] Y. Rong, C. Ji, Z. Wang, et al., J. Neuroinflammation 18 (2021) 196.
[12] M.S. Islam, H.Y. Shin, Y.J. Yoo, et al., Antioxidants 11 (2022) 1697.
[13] S.S.U. Hassan, S. Samanta, R. Dash, et al., Front. Pharmacol. 13 (2022) 1015835.
[14] N. Afroze, S. Pramodh, J. Shafarin, et al., Int. J. Mol. Sci. 23 (2022) 1707.
[15] Y. Long, X.Q. Li, J. Deng, et al., Ageing Res. Rev. 93 (2024) 102160.
[16] A.H. Shehata, A.F. Anter, S.M.N. Abdel Hafez, et al., Int. Immunopharmacol. 139 (2024) 112757.
[17] J. Li, Q. Long, H. Ding, et al., Adv. Sci. 11 (2024) e2308677.
[18] L. Gong, X. Zhang, K. Ge, et al., Biomaterials 267 (2021) 120483.
[19] G. Cheng, Y. Liu, R. Ma, et al., Nanomicro Lett. 14 (2022) 105.
[20] H.J. Liu, P. Xu, Adv. Drug Deliv. Rev. 191 (2022) 114619.
[21] S. Triarico, P. Maurizi, S. Mastrangelo, et al., Cancers 11 (2019) 824.
[22] D.F. Emerich, R.L. Dean, C. Osborn, et al., Clin. Pharmacokinet. 40 (2001) 105–123.
[23] H. Wu, Y. Wang, Z. Ren, et al., Chin. Chem. Lett. 36 (2025) 109996.
[24] D. Ribatti, V. Benagiano, D. Guidolin, Brain Sci. 13 (2023) 398.
[25] Y. Wang, S. Yuan, L. Zhou, et al., Int. J. Nanomedicine 20 (2025) 5059–5080.
[26] T. Zhu, Z. Chen, G. Jiang, et al., ACS Nano 17 (2023) 16770–16786.
[27] C. Xie, J. Liao, N. Zhang, et al., Chin. Chem. Lett. 35 (2024) 109149.
[28] M. Piffoux, A.K A Silva, C. Wilhelm, et al., ACS Nano 12 (2018) 6830–6842.
[29] V.M.R. Mythili, R.L. Rajendran, R. Arun, et al., Bioengineering 12 (2025) 92.
[30] Y. Xue, M. Gu, C. Chen, et al., Mol. Med. Rep. 27 (2023) 85.
[31] F. Branco, J. Cunha, M. Mendes, et al., ACS Nano 18 (2024) 16359–16394.
[32] X. Xue, X. Wang, M. Pang, et al., J. Nanobiotechn. 22 (2024) 196.
[33] M.A. Smith-Cohn, N.B. Burley, S.A. Grossman, Curr. Neuropharmacol. 20 (2022) 1383–1399.
[34] W. Hao, Y. Cui, Y. Fan, et al., J. Nanobiotechnology 19 (2021) 378.
[35] S. Jokar, I.A. Marques, S. Khazaei, et al., Bioengineering 9 (2022) 243.
[36] E.J. Park, M. Shimaoka, Methods Mol. Biol. 2668 (2023) 145–158.
[37] S.S. Palakurthi, B. Shah, S. Kapre, et al., Nanoscale Adv. 6 (2024) 5803–5826.
[38] B.K. Jung, K.Y. Ryu, Exp. Mol. Med. 55 (2023) 2138–2146.
[39] Q. Li, T.T. Wu, O.U. Akakuru, et al., Adv. Funct. Mater. 33 (2023) 2214826.
[40] P. Wen, Z. Sun, F. Gou, et al., Ageing Res. Rev. 104 (2025) 102667.
[41] M. Umar, S. Muzammil, M.A. Zahoor, et al., Evid. Based Complem. Alternat. Med. 2022 (2022) 1005255.
[42] H. Chew, V.A. Solomon, A.N. Fonteh, Front. Physiol. 11 (2020) 598.
[43] H. Yu, Q. Chang, T. Sun, et al., Ageing Res. Rev. 90 (2023) 102032.
[44] W.H. Chang, H.T. Hsu, C.C. Lin, et al., Int. J. Mol. Sci. 25 (2024) 2514.
[45] J. Li, Y. He, J. Fu, et al., Front. Nutr. 9 (2023) 1121789.
[46] Q. Zheng, H. Liu, H. Zhang, et al., Adv. Sci. 10 (2023) e2300758.
[47] F. Hemmati, N. Valian, A. Ahmadiani, et al., Iran. J. Pharm. Res. 23 (2024) e144200.
[48] F.S. Mohammed, S.B. Omay, K.N. Sheth, et al., Expert Opin. Drug Deliv. 20 (2023) 55–73.
[49] F.Q. Zhang, J.L. Jiang, J.T. Zhang, et al., Neural Regen. Res. 15 (2020) 242–250.
[50] D.H. Jung, M.E. Pak, H.J. Lee, et al., Life 10 (2020) 240.
[51] S.S. Elshama, M. El-Kenawy Ael, H.E. Osman, Iran. J. Basic Med. Sci. 19 (2016) 712–719.
[52] E. Domi, F.F. Caputi, P. Romualdi, et al., J. Neurosci. 39 (2019) 9864–9875.
[53] Y. Yin, T. Ju, D. Zeng, et al., Pharmacol. Res. 207 (2024) 107322.
[54] M. Ishiyama, H. Gotoh, S. Oe, et al., Mol. Neurobiol. 62 (2025) 1373–1387.
[55] C. Zhao, C. Gao, Z. Yang, et al., Chin. Chem. Lett. 36 (2025) 111089.
[56] S. Matsui, T. Sasaki, D. Kohno, et al., Nat. Commun. 9 (2018) 4604.